

# Computing 3D Mesh Correspondence for Aortic Root Shape Modelling

Robert Palmer<sup>1</sup>  
526844@swansea.ac.uk

Gary Tam<sup>1</sup>  
K.L.Tam@swansea.ac.uk

Xianghua Xie<sup>1</sup>  
X.Xie@swansea.ac.uk

Rob Alock<sup>2</sup>  
robalcock@doctors.org.uk

Carl Roobottom<sup>3</sup>  
carl.roobottom@nhs.net

<sup>1</sup> Department of Computer Science  
Swansea University, UK  
<http://csvision.swan.ac.uk>

<sup>2</sup> Peninsular Radiology Academy Plymouth Hospitals NHS Trust, UK

<sup>3</sup> Plymouth University Schools of Medicine & Dentistry Plymouth Hospitals NHS Trust, UK

---

## Abstract

Aortic valve disorder is one of the common diseases affecting elderly people. To provide visual assessment and improve success of surgical treatment, a segmentation technique equipped with a reliable statistical shape model is required. This in turn requires reliable dense correspondences establishment. This paper develops a reliable 3D registration technique targeting aortic region. Given a few easily identifiable landmark correspondences, our technique obtains a much denser set of point correspondences across a set of 3D aortic sources meshes to the target mesh. We propose to use geodesic interpolation, a new mesh based similarity metric, and a two-stage local transformation to develop a better registration technique for 3D aortic meshes. It results in better correspondences compared to existing work, shows an average Hausdorff distance of  $3.65\text{mm}$  and point-to-mesh distance of  $0.41\text{mm}$ . Visual comparison is also provided to assess the quality of the point correspondences.

## 1 Introduction

Aortic valve disorder is one of the valvular heart diseases common among elderly people affecting 3% of global population. Lots of the cases of aortic diseases often require surgical treatment. A non-invasive segmentation technique, which is capable to segment and visualise the 3D aortic valve and root region from volumetric medical images, is essential to patient pre-selection, planning and post-evaluation of surgical result. The development of such a non-invasive segmentation technique is challenging because of the wide difference in the shapes of 3D aortic regions among patients. Most literatures use statistical shape models (SSM) to provide prior knowledge to constraint the possible shape space trained from training samples. To build a SSM, a set of segmentation of training 3D shapes, and their

corresponding landmarks surface points are required. Manually segment and label all correspondences across all training 3D shapes is a time-consuming and tedious process. Here, we try to develop a semi-automatic technique for obtaining a good set of point correspondences.

A number of approaches to find correspondences in anatomical shapes have been proposed, many of which work directly on the meshes themselves. These include [10, 11, 12, 13]. However, most of these techniques establishes only a set of sparse correspondences. Our observation is that this is useful to characterise the regions of shapes close to these landmarks correspondences, but not those that are far away. These often lead to an SSM that inadequately describes the difference among the shapes. This is particular true for 3D aortic data where only a few landmarks can be easily identified. Our ideas in this paper is to obtain a denser set of corresponding landmarks through (a) interpolation by geodesic distances, (b) a new mesh based similarity metric two-stage local transformation following the earlier work of [14]. As demonstrated in our experiment, our technique can find point correspondences among aortic shapes better than [14].

## 2 Method

This section describes how to find a dense set of landmark correspondences across a set of triangular training meshes. A target mesh  $M_t = (V_t, E_t, F_t)$  with  $|V_t| = n$  vertices is selected from the mesh set, and the remaining meshes are regarded as the source meshes. Assume there is a source mesh  $M_s = (V_s, E_s, F_s)$  where  $|V_s| = p$ , and  $n \neq p$ , and  $m$  manually labelled corresponding landmark points on both meshes such that  $P_t \subset V_t$  and  $P_s \subset V_s$ , where  $m \ll n$ , the problem now is to find a complete set of  $n$  vertex correspondences on the source mesh  $M_s$ . Our method obtains a set of source vertices  $Q_s \subset V_s$  that are correspondent with  $V_t$ .

Our method is similar to that of Frangi *et al.* [15]: 1) estimates a global affine transformation through the manually labelled landmark correspondences, and aligns all meshes into a *natural coordinate system*; 2) estimates local non-rigid transformation through free-form-deformation (FFD) and aligns the source meshes to target; 3) finds a complete set of correspondences by nearest neighbour search. Our work innovates in three ways: a) before applying global transformation, we interpolate a denser set of correspondences through geodesic interpolation; b) instead of using image-based similarity metric [15], we define a mesh-based similarity metric instead; c) we employ a coarse-to-fine strategy to define our two-stage local transformation.

### 2.1 Input and Geodesic interpolation

Each aortic root mesh was labelled with 10 corresponding landmark points. Three of these were aortic valve *hinge points*; the first of which was the nearest to the *aortic arch*, with the remaining two labelled in a clockwise fashion. Three *commissure points* were labelled between the hinges, with the first commissure point between hinges 1 and 2, and the remaining labelled in a clockwise fashion. Three points were labelled on the *sinotubular junction*, directly below the three hinge points. The first of which was below the first hinge point, with the remaining two once again labelled in a clockwise fashion. Finally, a *centre point* was labelled on the surface at the centre of the root (see Figure 1 (left)).

Using the 10 landmarks, a denser set of corresponding landmarks were found using an interpolation approach. Pairs of landmark points were defined and the surface paths between them were determined using Dijkstra’s shortest path algorithm. Fifteen paths were

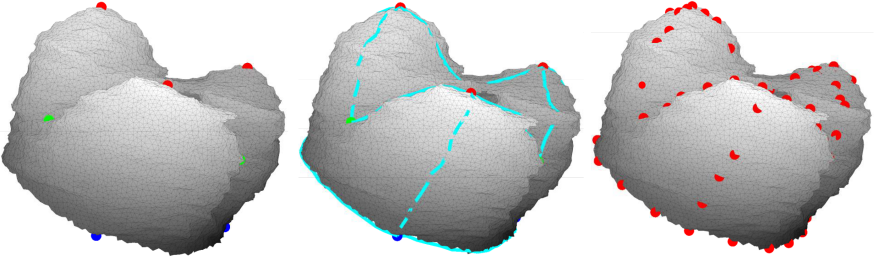


Figure 1: Initial landmark labelling. (left) Initial sparse landmark points showing the *hinges* (red), *commissures* (green), and *sinotubular junction points* (blue); (middle) Interpolation paths between pairs of initial landmarks; (right) New landmarks after path interpolation.

determined in all; six between the hinge points and their nearest commissure points, three between the hinge points and the centre point, three between the hinge points and their corresponding sinotubular junction points, and three between the sinotubular junction points. 5 evenly spaced points were then interpolated along each path, leaving a total of 65 landmark points. Figure 1 (middle) shows the interpolation paths and (right) the new landmark points.

## 2.2 Transformation Estimation

Let  $T(x, y, z)$  be the transformation that deforms mesh  $M_s$  so that  $T : M_s \mapsto M_t$ . It consists of a global affine transformation, followed by two local transformations.

$$T(x, y, z) = T_g(x, y, z) + [T_{l_1}^{H_1}(x, y, z) + T_{l_2}^{H_2}(x, y, z)] \quad (1)$$

The global transformation  $T_g$  accounts for the global alignment between the source  $M_s$  and target  $M_t$  meshes. Similar to [2], we estimate an affine transformation using the denser set of landmark points to align  $P_s$  to  $P_t$  (results from Section 2.1).

To allow a more flexible matching between the source and target meshes, a local transformation  $T_l$  is also estimated based on B-spline FFD. Our approach estimates  $T_l$  in two separate stages; a coarser transformation  $T_{l_1}$ , followed by a finer transformation  $T_{l_2}$ . For both cases, the FFDs themselves are also estimated using a multi-resolutional procedure  $T_l^H$ , where  $H$  is the number of mesh resolutions [2, 3, 4].

$$T_l^H(x, y, z) = \sum_{h=1}^H T_l^h(x, y, z) \quad (2)$$

At each mesh resolution  $h$ , the voxel lattice is warped by moving a set of voxel lattice control points  $\phi_{i,j,k}^h$  of size  $[n_x \times n_y \times n_z]$ , and an FFD is estimated [3, 4]. These control points act as parameters of the B-spline FFD. If  $\delta_0$  is the original control point spacing, then at each resolution  $h$ , the spacing is defined as  $\delta_h = \delta_0/2^h$ . Decreasing  $\delta_0$  decreases the flexibility of the spline, whereas increasing  $\delta_0$  allows a more local deformation. The FFD is defined as

$$T_l^h(x, y, z) = \sum_{l=0}^3 \sum_{m=0}^3 \sum_{n=0}^3 B_l(u)B_m(v)B_n(w)\phi_{i+l,j+m,k+n}^h \quad (3)$$

where  $B_l$  represents the  $l$ th basis function of the cubic B-spline [3, 4], and  $i = \lfloor x/n_x \rfloor - 1$ ,  $j = \lfloor y/n_y \rfloor - 1$ ,  $k = \lfloor z/n_z \rfloor - 1$ ,  $u = x/n_x - \lfloor x/n_x \rfloor$ ,  $v = y/n_y - \lfloor y/n_y \rfloor$ , and  $w = z/n_z - \lfloor z/n_z \rfloor$ . The

B-spline parameters  $\phi_{i,j,k}^h$  are optimised using gradient descent with the objective function  $E(\phi) = E_s(\text{target}, \text{source}) + \lambda E_r(T_i)$ , where  $E_r$  is a smoothness cost and  $\lambda$  is a regularisation term.  $E_s$  is a similarity metric based on the sum-of-squared-distance (SSD) measure between sets of mesh vertices. The transformations are applied sequentially. First  $T_{i_1}$  is estimated and applied to  $M_s$  to get  $M'_s$ .  $T_{i_2}$  is then estimated and applied to  $M'_s$  to get  $M''_s$ .

Differs from existing approach, we apply the above FFD transformation in a two-stage process through  $T_{i_1}$  and  $T_{i_2}$ .  $T_{i_1}$  is a coarser transformation than  $T_{i_2}$ . The intuition is that the first local transformation  $T_{i_1}$  provides a better alignment between the overall structure of the two meshes. Once the meshes are aligned, a local transformation  $T_{i_2}$  with a higher resolution is used. This alleviates over-fitting problem, avoids sharp peaks or troughs in the surface of the meshes, while reduces the chance of edge overlapping.

Two factors contribute to making  $T_{i_1}$  a coarser transformation than  $T_{i_2}$ . The first is the similarity metric calculation. For  $T_{i_1}$  this is estimated from the SSD between the sparse landmarks  $P_s$  and  $P_t$ . The similarity metric for  $T_{i_2}$  however is based on the SSD between *all* vertices in  $V'_s$  and  $V_t$ . The other factor is the control point spacing  $\delta_0$ , during FFD estimation.  $T_{i_1}$  has spacing of  $\delta_{0_1}$ , and  $T_{i_2}$  has spacing of  $\delta_{0_2}$ , where  $\delta_{0_1} > \delta_{0_2}$ . For our estimation of  $T_{i_1}$  we decided to use  $H_1 = 3$  mesh resolutions, and an initial control point spacing of  $\delta_0 = 15\text{mm}$ . A relatively large  $\delta_0$  was selected here as to suppress the amount of local deformation as the FFD was estimated using the sparse set of corresponding landmarks.  $H_2 = 3$  was also used for the estimation of  $T_{i_2}$ , however here we decided to use  $\delta_0 = 5\text{mm}$  in order to capture a more local deformation by giving the FFD more degrees of freedom.

### 2.3 Finding Complete Correspondence

Once the source has been deformed to  $M''_s$  and properly aligned to  $M_t$ , establishing point correspondences between two similar shapes becomes simpler. We apply simple nearest neighbour algorithm to find complete point correspondences. For *every* vertex in  $V_t$ , the nearest neighbour based on Euclidean distance is found in  $V''_s$ . The nearest neighbour in  $V''_s$  is considered the corresponding vertex, and this leads to a new set of re-ordered deformed source vertices  $Q'_s$ . Finally, the inverse local transformation  $(T_{i_1} + T_{i_2})^{-1}$  is applied to  $Q'_s$  to get the complete source correspondences  $Q_s$  in the *natural coordinate system*.

## 3 Results

An experiment was conducted using 37 aortic root meshes, where each mesh was used as the target in a leave-one-out fashion. The aortic root, including the ascending aorta and aortic arch were labelled in CT TAVI images, of size  $[512 \times 512 \times (500 - 800)]$ , and voxel size was  $[0.48\text{mm} \times 0.48\text{mm} \times 0.62\text{mm}]$ . In order to ensure that the hinges were clearly seen, multi-planar-rotation software was used during image labelling. This was followed by the marching-cubes algorithm for mesh generation, and the 10 landmarks (3 hinges, 3 commissures, 3 sinotubular junction points and a root centre point) were manually labelled. The ascending aorta and aortic arch were then discarded from the meshes below the plane on which the 3 sinotubular junction points lay. The average local mesh size was  $[34.46 \pm 5.56\text{mm} \times 34.19 \pm 4.04\text{mm} \times 24.02 \pm 3.98\text{mm}]$ .

Registration of source to target was evaluated using the mean symmetrical Hausdorff distance  $H_{dist}$ , and mean point-to-mesh distance  $Epm_{dist}$  between  $M_t$  and  $M''_s$ . The results were  $H_{dist} = 3.65 \pm 1.19\text{mm}$  and  $Epm_{dist} = 0.41 \pm 0.25\text{mm}$ . This represents a mean distance

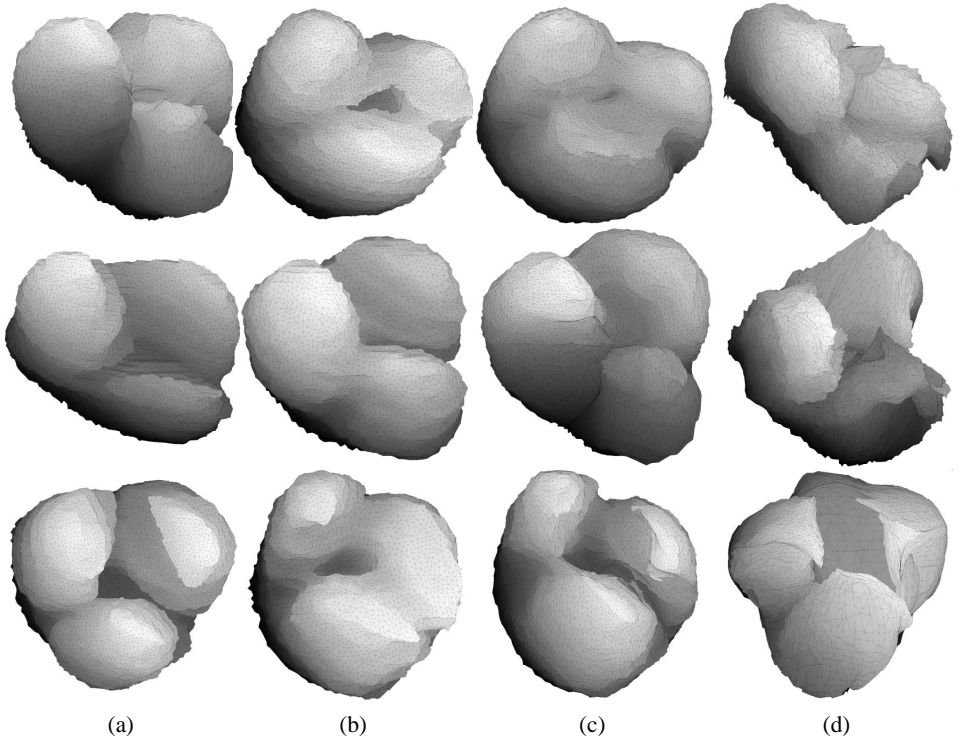


Figure 2: Deformation comparison. (a) source meshes; (b) target meshes; (c) our estimation; (d) results from image based technique [1].

error of  $<1$  voxel, and a deformed mesh with no distant outlying vertices from the surface. Figure 2 compares the deformation of source to target using an image-based metric [1, 5], and our method using the mesh-based approach. This shows that our method deforms the source meshes so that they have a greater visual resemblance to the target than the deformed meshes using image-based transformation estimation. In addition, the resulting meshes using our method have no compressed or stretched mesh faces, and no tangled mesh edges, leaving a smooth, regularized mesh. This is in contrast to the deformed meshes using an image-based similarity metric, where the meshes appear stretched and compressed in numerous areas.

The close similarity in appearance between  $M_t$  and  $M_s''$  allowed more accurate corresponding vertices to be found using the nearest-neighbour calculation. Figure 3 compares the vertex correspondences using our method, and the image-based technique [1].

## 4 Conclusion

We have presented a semi-automatic method for finding complete vertex correspondence from a set of sparsely spaced corresponding landmarks across a set of 3D meshes of aortic regions. In particular, we have demonstrated this method using complex aortic root meshes, which have corresponding images with varying appearance. This data is challenging to existing techniques like [1]. Future work will focus on building accurate SSMs using these

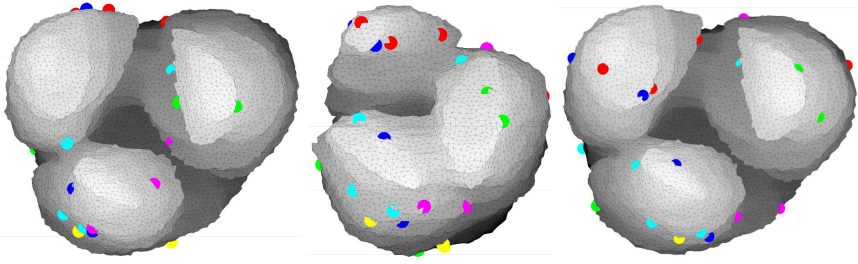


Figure 3: Visual comparison of vertex correspondences (left) image-based transformation estimation; (middle) target mesh; (right) our results.

corresponding vertices, and implementing the statistical model in a fully-automatic aortic root segmentation technique.

## Acknowledgement

The authors would like to thank Feng Zhao and Jingjing Deng for their generous help in preparing the dataset groundtruth. We also would like to acknowledge Daniel Rueckert for the Image Registration Toolkit (<https://www.doc.ic.ac.uk/~dr/software/>).

## References

- [1] A. D. Brett and C. J. Taylor. A method of automated landmark generation for automated 3d pdm construction. *Image and Vision Computing*, 18(9):739–748, 1999.
- [2] A. F. Frangi, D. Rueckert, J. A. Schnabel, and W. J. Niessen. Automatic construction of multiple-object three-dimensional statistical shape models: Application to cardiac modeling. *Transactions On Medical Imaging*, 21(9):1151–1166, 2002.
- [3] S. Lee, G. Wolberg, K. Y. Chwa, and S. Y. Shin. Image metamorphosis with scattered feature constraints. *Transactions on Visualization and Computer Graphics*, 2(4):337–354, 1996.
- [4] S. Lee, G. Wolberg, and S Y. Shin. Scattered data interpolation with multilevel b-splines. *Transactions on Visualization and Computer Graphics*, 3(3), 1997.
- [5] D. Rueckert, L. I. Sonoda, C. Hayes, D. Hill, M. O. Leach, and D. J. Hawkes. Nonrigid registration using free-form deformations: Application to breast mr images. *Transactions on Medical Imaging*, 18(8):712–721, 1999.
- [6] D. Rueckert, A. F. Frangi, and J. A. Schnabel. Automatic construction of 3-d statistical deformation models of the brain using nonrigid registration. *Transactions on Medical Imaging*, 22(8):1014–1025, 2003.
- [7] G. Subsol, J. P. Thirion, and N. Ayache. A scheme for automatically building three-dimensional morphometric anatomical atlases: Application to a skull. *Medical Image Analysis*, 2(1):37–60, 1998.
- [8] Y. Wang, B. S. Peterson, and L. H. Staib. Shape-based 3d surface correspondence using geodesics and local geometry. *Pattern Analysis and Machine Intelligence*, 22(7):738–743, 2000.